A Framework to Calibrate the Scanning Electron Microscope under Variational Magnifications

Xingjian Liu, Zhongwei Li, Pedro Miraldo, Kai Zhong, and Yusheng Shi

***Abstract*—We propose and demonstrate a new and effective framework to calibrate the Scanning Electron Microscope (SEM), under variational magnifications from 20 to 500. Unlike previous approaches that required different models and calibration procedures for different magnifications, this framework regards the SEM as a black box. The general imaging model is first introduced in modeling the SEM system, to explore the nature of SEM imaging. In order to relax the complexity of the general imaging model and calibration process, the smooth general imaging model and a linear point-based calibration method is developed. The experimental results well agree with the theoretical predication and show great potential to realize SEM calibration.**

***Index Terms*—Scanning electron microscope, Calibration, Computational imaging, General imaging model.**

I. Introduction

THE Scanning Electron Microscope (SEM) has been a valuable resource for viewing samples at high resolution and depth of field [1]. It is an essential instrument to observe, analyze, and manipulate micro and nano specimens with micro-scale and nano-scale accuracy. The imaging process of a SEM is essentially different from a light microscope. The light microscope turns light information to 2D information to form the images. A SEM system contains an electron gun to supply the electrons that forms an electron beam. As shown in Fig. 1, the electron beam scans across the specimen surface and collects back scattered (or secondary) electrons, using a fixed detector to construct the image. The SEM is designed for visualization. It also has been used for some metrological studies and vision-based applications, such as: nano-scale 3D reconstruction [2], nanomanipulation [3], micro or nano-scale deformation measurement [4]. In the above applications, the computation of metric information from 2D SEM images is needed. Therefore, the SEM's imaging model and its calibration become crucial issues to be considered.

In earlier studies, two different imaging models were used to conduct SEM calibration, according to the SEMs magnifications [5]. At low magnification, since the field of view and the angular view are large, the pinhole model was applied. On the other hand, at high magnification the field of view and the angular field of view are both very small. The parallel projection was recommended. However, different researchers had different views about the magnification limit for the choice of pinhole model and parallel projection model [5], [6], [7]. Generally, the limit is chosen between 200× and 1000× or higher [5], [6]. According to Hemmleb et al. [7], the magnification limit for pinhole model was about 500×. The applied law of projection should be changed at magnifications higher than 500×, from pinhole to parallel model. Sutton et al. [8] claimed that the approximation of the pinhole model by the parallel projection does not seem adequate lower than a magnification 20000×.

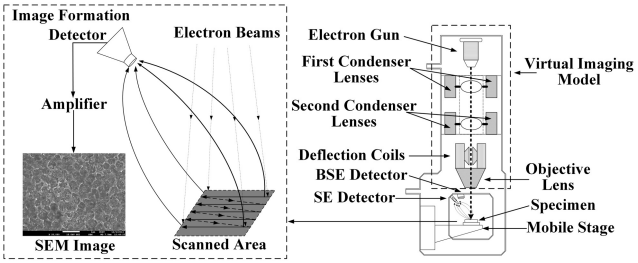

Fig. 1. Diagram representing the funcionality of a Scanning Electron Microscope (SEM).

As for the calibration of the SEM, several methods and optimization algorithms were proposed, e.g. [9], [10], [11]. Ritter et al. [9] developed a landmark-based 3D calibration strategy. In the process, a few SEM images of 3D micrometre-sized reference structure, with the shape of a cascade slope-step pyramid, were taken in order to conduct the calibration. However, the fabrication of this special 3D reference structure is an important and difficult issue. To realize a smoothly switch between the low magnification and high magnification, Malti et al. [10] porposed a systematic method of estimating the static distortion and the projective mapping, in a continuous range of magnification scale. Cui and Marchand [11] proposed a novel approach of SEM calibration, based on projection model and a non-linear minimization process. However, the spatial distortion parameters (skewness, radial distortion and spiral distortion) were eliminated in their experiments.

Existing calibration methods, as stated above, mostly used optical parametric imaging models to calibrate the SEM. However, SEM is a complex imaging system, which is essentially different from an optical system. Therefore, it becames difficult to evaluate the calibration results. To calibrate complex imaging system, Grossberg and Nayar [12] defined a nonparametric discrete imaging model, called general imaging model. Differently from the usual parametric imaging models, this model consists of the individual association between pixels

This work was supported by the National Natural Science Foundation of China (51205149), the Science and Technology Planning Project of ShehZhen, China (JCYJ20050630155150209).

X. Liu, Z. Li, K. Zhong and Y. Shi are with the State Key Laboratory of Material Processing and Die & Mould Technology, Huazhong University of Science and Technology, Wuhan 430074, China. e-mail: (zwli@hust.edu.cn).

P. Miraldo is with Institute for Systems and Robotics (LARSyS), Instituto Superior Tcnico, Lisboa, Avenida Rovisco Pais, 1, 1049-001 Lisboa, Portugal.

This article has been accepted for publication in a future issue of this journal, but has not been fully edited. Content may change prior to final publication. Citation information: DOI 10.1109/LPT.2016.2522758, IEEE Photonics Technology Letters

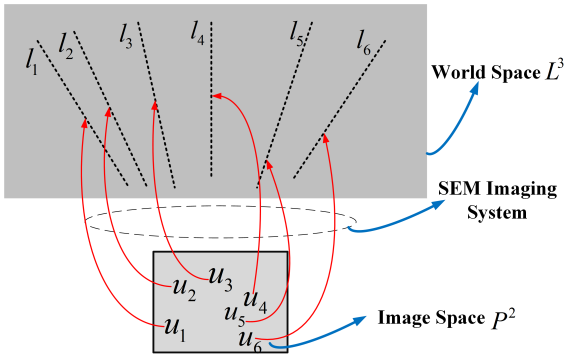

Fig. 2. Representation of the general imaging model used in this paper, to model the SEM imaging system.

and rays in 3D space. In addition, they also proposed a simple ray-based calibration method which required several calibration pattern, with known structure and motions between the acquisitions. Sturm and Ramalingam [13] proposed a general calibration technique, that required three images of a calibration pattern, from arbitrary and unknown viewing positions. Miraldo and Araujo [14] changed the general imaging model using radial basis functions, to interpolate image coordinates and 3D lines, allowing both an increase in resolution (due to their continuous nature) and a more compact representation.

Based on the above analyses, it is a tremendous challenge to represent the SEM imaging process well under variational magnifications. The research of the general imaging model gives us some inspiration about SEM imaging process modeling. We creatively address the problem of exploring the nature of SEM imaging process using general imaging model, where the SEM can be seen as a black box connecting pixels with corresponding rays. To the best of our knowledge, it is the first time to establish the SEM model by using general imaging model. The imaging model of the SEM, under different magnifications from 20 to 500, is revealed. A new framework to calibrate the SEM is developed, which is the main contribution of the paper when compared with previous approaches. To allow the simplification of the general calibration procedure and the parametric representation, the smooth general model and a linear point-based calibration method are developed. Then, the residual of the smooth model is analyzed and compared with traditional pinhole model with a nonlinear optimization.

II. SMOOTH GENERAL MODEL OF THE SEM

An imaging system represented by the general imaging model, can be seen as a set of associations between the incoming rays (light or electron from the 3D world space) and the pixels in 2D image space. In this sense, we regard SEM system as a black box, represented by the general imaging model, which gives the corresponding relationship between all image pixels $\mathbf{u} \in \mathcal{P}^2$ and the incoming (chief) ray $\mathbf{l} \in \mathcal{L}^3$, as shown in Fig. 2. Here, $\mathcal{P}^2$ represents the image space and $\mathcal{L}^3$ represents line space world space. Most of previous research of general imaging model are discrete and non-parametric [12], [13]. These models require the use of mapping arrays to calibrate the imaging model. The image pixels have associated a set of parameters that are independent from their neighbors. Therefore, performing a complete camera calibration requires setting the mapping parameters for every pixel. For each pixel, there are seven unknown parameters to be computed. For an image with size $N \times M$, there are $7NM$ unknown parameters to be computed. At the same time, errors may easily appear while fitting a specific pixel-line relationship from the neighbor discrete ones. Hence, there are many difficulties to conduct SEM calibration with complex traditional general models, such as the image noise, the manufacture of small-scale 3D calibration target, the fitting errors etc. It is well established that a SEM imaging system has pixel-line relationships vary smoothly along the image. So, in order to relax the complexity of the general imaging model and calibration process, we use a smooth general imaging model [14] to represent the nature of SEM imaging process. Basically, we use the assumption that the pixel-line mappings can be represented by a smoothly varying vector-valued function $\mathbf{f} : \mathcal{P}^2 \sim \mathcal{L}^3$, that maps a point in the image plane to a line in 3D space. This assumption significantly decreases the number of model unknowns and also allows us to filter out some errors due to noise. Using this assumption, one can define the smooth camera model as vector-valued function:

$$\mathbf{l} \sim \mathbf{s}(\mathbf{u}) = \underbrace{\left[\ \boldsymbol{\phi}(\mathbf{u}) \ \middle|\ \mathbf{q}(\mathbf{u})\ \right]_{1\times(P+3)}}_{\mathbf{r}(\mathbf{u})} \mathbf{H}_{(P+3)\times 6} \tag{1}$$

where: $\mathbf{l}$ represents a 3D line while $\mathbf{s}(\mathbf{u})$ contains six elements to represent the line's four degrees of freedom in Plucker coordinates. $\mathbf{H}$ are the model's unknown parameters; $\mathbf{q}(\mathbf{u}) = \left[\ 1 \ \middle|\ \mathbf{u}\ \right]_{1\times 3}$; and $\phi_i(\mathbf{u}) = \phi(|\mathbf{u} - \mathbf{c}_i|)$, where $\mathbf{c}_i$ are a set of pre-defined image control points (for more information see [14]). $\phi(.)$ denotes a radial basis function (Miraldo and Araujo argue that *gaussian* and *multi-quadrics* are suitable radial basis functions, special due to calibration issues).

One of the most important features of the smooth camera model is related with the respective calibration procedure which, in this case, consists in the estaimtin of the parameters of the matrix $\mathbf{H}$. Contrarily to the other general camera model, which required the estimation of the 3D projection ray for all pixel (they required at least two 3D points in the world for each pixel), this method takes the advantage of the smoothness to allow an easier point-based calibration procedure that does not require more than one 3D points for only a subset image pixels (much less than the total number of pixels). This calibration procedure is then much easier than the calibration of general camera models and, since SEM is a smooth imaging device, suitable for the proposed framework. To conclude, from a set of patchings between image pixels and 3D points $\{\mathbf{p}_i \mapsto \mathbf{x}_i\}$, the unknown parameters (camera calibration) can be easily computed using the following equations:

$$\begin{bmatrix} \mathbf{Q}(\mathbf{p}_1) \otimes \mathbf{r}(\mathbf{x}_1) \\ \mathbf{Q}(\mathbf{p}_2) \otimes \mathbf{r}(\mathbf{x}_2) \\ \vdots \\ \mathbf{Q}(\mathbf{p}_N) \otimes \mathbf{r}(\mathbf{x}_N) \end{bmatrix} \text{vec}(\mathbf{H}) = \mathbf{0}, \quad \text{and} \quad \mathbf{Q}(\mathbf{p}_i) = \begin{bmatrix} \widehat{\mathbf{p}}_i & -\mathbf{I} \\ \mathbf{0} & \mathbf{p}_i^T \end{bmatrix}_{4\times 4}, \tag{2}$$

This article has been accepted for publication in a future issue of this journal, but has not been fully edited. Content may change prior to final publication. Citation information: DOI 10.1109/LPT.2016.2522758, IEEE Photonics Technology Letters

where: $\otimes$ denotes the kronecker product; vec $(\mathbf{A})$ denotes the stacking of the columns of $\mathbf{A}$; and $\widehat{\mathbf{p}}_i$ is the 3×3 anti-symmetric matrix that linearizes the cross product, such that $\mathbf{a} \times \mathbf{b} = \widehat{\mathbf{a}}\,\mathbf{b}$.

III. EXPERIMENT RESULTS AND DISCUSSION

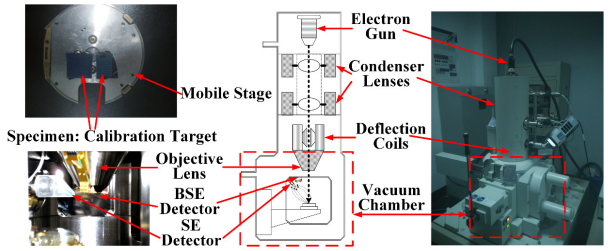

Fig. 3. The JSM-7600 SEM manufactured by JEOL.

The SEM that has been used to validate the general imaging model and calibration experiment is a JSM-7600 SEM manufactured by JEOL, as shown in Fig. 3. The electron gun is equipped with a tungsten filament that can support acceleration voltage from 0.1kv∼30kv. The magnification of the SEM is from 25 to 1,000,000 and the digital image resolution that can be changed among 1,280 $\times$ 960 pixels, 2,560 $\times$ 1,920 pixels and 5,120 $\times$ 3,840 pixels. Also, it provides a 6-DOF platform including 360° rotation and tilt from -5°∼$+70^\circ$. In our experiment, the SEM images have a size of 1,280 $\times$ 960 pixels and the acceleration voltage is 15kv. And a nano-positioning table is placed on the platform where the calibration target was attached on. Its range of motion and resolution are 1500 μm and 0.03μm respectively.

A multi-scale planar calibration target is designed and the photolithography method is used to manufacture it. The precision of the method can reach to $\pm 0.05\mu$m. It is a hierarchy of circle arrays where distance between adjacent centers of circle are of 20μm, 30μm, 50μm and 90μm, as shown in Fig. 4. The acquired SEM images magnification ranges from $\times$75 to $\times$500. Then the precise localization of circles centers is detected and ordered. Fig. 5 presents the calibration procedure where the 3D points data used for the calibration are generated from moving the nano-positioning table. The calibration target is first attached to the table. We regard the target as the x-o-y plane and the original point is at the center of the target. Then it is translated 6 times, as shown in Fig. 5(a). The translation distance between adjacent positions is 200μm. while the nano-positioning table moving, the working distance always remained 9mm to avoid the influence of beam deflection voltage changing. Fig. 5(b) displays the image points (black squares) and control points (red dots) used in the calibration process.

We introduce a parameter called point-line distance error to present the accuracy of a imaging model. As the Fig. 6(a) shows, for given imaging model, we can calculate a lines equation l_u that is corresponding to a given image point u_{pixel}. If the corresponding ground-truth world point u_{world} is known, then we can calculate the line-point distance between the world point u_{world} and the line l_u. The distance is smaller, the model

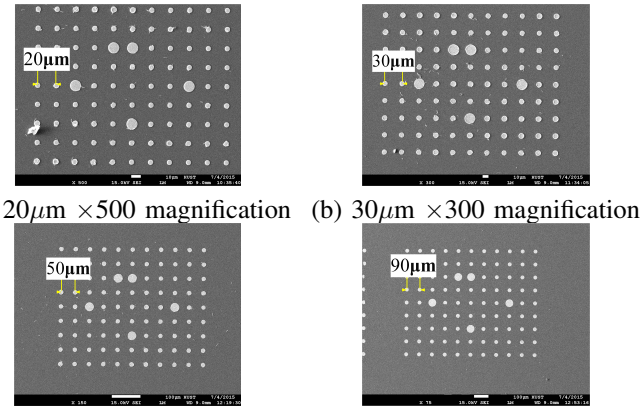

(a) 20μm $\times$500 magnification (b) 30μm $\times$300 magnification

(c) 50μm $\times$150 magnification (d) 90μm $\times$75 magnification

Fig. 4. Multi-scale calibration planar size from 30μm to 90μm.

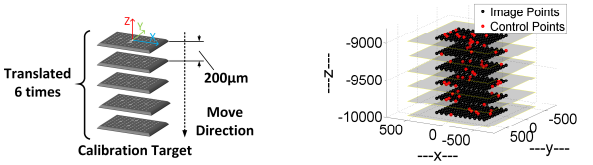

(a) translating the target 6 times along Z-axis

(b) image points and control points

Fig. 5. Calibration procedure

is more accurate. In our smooth general model, *Gaussian* and *Multi-quadrics* are suitable radial basis functions, special due to calibration issues [14]. Fig. 6(b) shows the evaluation of the average point-line distance error as a function of the number of control points for the two different radial basis functions under 400 magnification. It demonstrate that *Multi-quadrics* is more suitable choice of radial basis function for SEM imaging system and increasing the control points will reduce the average point-line distance errors. In the following experiment, we choose *Multi-quadrics* as the radial basis function with 60 control points.

Fig. 7 shows the results of the calibration under four different magnifications that are $\times$75, $\times$150, $\times$300 and $\times$500. Under low magnifications, the estimated lines almost converge at one point and it is very close to a pinhole model. As the magnification increases, the estimated lines become more diverging and they do not converge at former point under 500 magnification. To some extent, the focal length becomes longer. So high magnification may bring very large focal length and the model would be close to a parallel model as

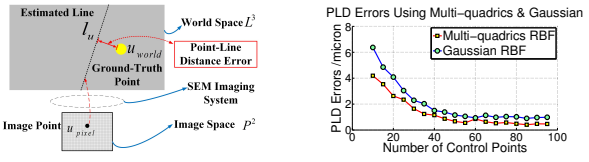

(a) Definition of point-line distance error

(b) Evaluation of the average point-line distance error

Fig. 6. Point-line distance error and its evaluation as a function of the number of control point

This article has been accepted for publication in a future issue of this journal, but has not been fully edited. Content may change prior to final publication. Citation information: DOI 10.1109/LPT.2016.2522758, IEEE Photonics Technology Letters

the former research argued [5], [6], [7], [8].

To validate the further effectiveness of our smooth general model, the residual of the general imaging model is analyzed and compared to the traditional pinhole model [15]. The tsai's method with nonlinear optimization is used to calculate the parameters of pinhole model [15]. The magnification changes from $\times 75$ to $\times 500$. And the corresponding target types are 90μm, 70μm, 50μm, 40μm, 30μm, 20μm respectively where the distances between adjacent centers of circle represent the target types. As shown in Fig. 8(a), the average line-point distance under low magnification is higher compared with high magnification for both the two models. We think that the pixel resolution primarily causes this. Under low magnification of $\times 75$, the pixel resolution is low which is about 1.235μm/pixel compared with 0.185μm/pixel under $\times 500$ magnification. But the precision (in pixel) of the center detection algorithm is same for every SEM images. Therefore, the absolute point-line error is higher under low magnification. To further avoid the effect of pixel resolution, we report the point line distance errors as a percentage of the horizontal field width(HFW) as shown in Fig. 8(b) while the horizontal field width was calculated by scale factor of the SEM images. The percentage of the error is still below 0.5% for the both two models. They increase slightly as the magnification changing, because the horizontal field of width falls a little bit faster compared with the pixel resolution raising. In our experiment, we calibrate specific magnifications. Therefore, it will lead to 1-3% relative interpolation error while interpolating between different magnifications just as traditional methods hold. However, we advise to calibrate the model for a specific magnification firstly before a specific SEM vision-based task such as micro or nano-manipulation. In this papaer, the magnifications range is between $\times 75$ to $\times 500$. The experiment results demonstrate that our smooth general imaging model for SEM is practically effective and its principle is much closer to the SEM imaging theory than traditional ones'. Our future work will focus on the reduction of interpolation errors between different magnifications and attempting to add the magnification factor into the SEM imaging model. If the magnification factor could be added into the smooth general model as a control factor, we can build a magnification-depended imaging model. Also, other factors that affect the model parameters can be added into the model as control factors. Therefore, the interpolation problem may be solved in a reliable way.

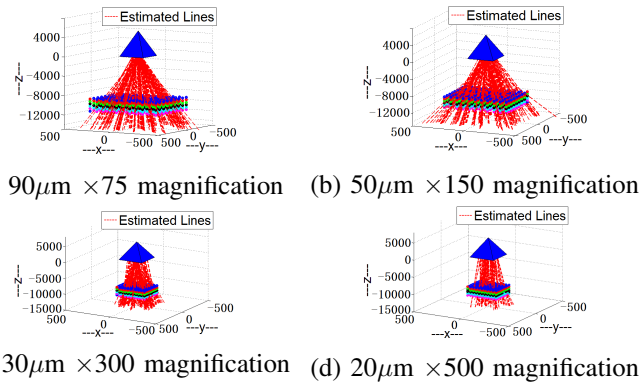

(a) 90μm $\times 75$ magnification (b) 50μm $\times 150$ magnification

(c) 30μm $\times 300$ magnification (d) 20μm $\times 500$ magnification

Fig. 7. Multi-scale calibration Results.

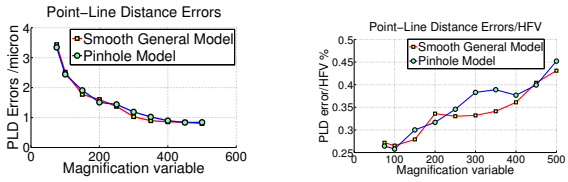

(a) Evaluation of the average point-line distance error

(b) Evaluation of the average point-line distance error as a percentage of the horizontal field width(HFW)

Fig. 8. Evaluation of the point line distance error and the error as a percentage of the horizontal field width(HFW)

REFERENCES

[1] L. Reimer, "Scanning electron microscopy: physics of image formation and microanalysis," *Measurement Science and Technology*, vol. 11, no. 12, p. 1826, 2000.

[2] L. B. Rad, H. Feng, J. Ye, and R. Pease, "Computational scanning electron microscopy," in *International Conference on Frontiers of Characterization and Metrology*, vol. 931, no. 1, 2007, pp. 512–517.

[3] C. Ru and L. Sun, "Note: Mechanical and electrical characterization of nanowires in scanning electron microscope," *Review of Scientific Instruments*, vol. 82, no. 10, p. 106105, 2011.

[4] T. Zhu, M. A. Sutton, N. Li, J.-J. Orteu, N. Cornille, X. Li, and A. P. Reynolds, "Quantitative stereovision in a scanning electron microscope," *Experimental Mechanics*, vol. 51, no. 1, pp. 97–109, 2011.

[5] N. Cornille, "Accurate 3d shape and displacement measurement using a scanning electron microscope," Ph.D. dissertation, University of South Carolina, 2005.

[6] M. Ritter, M. Hemmleb, B. Lich, P. Faber, and H. Hohenberg, "Sem/fib stage calibration with photogrammetric methods," in *ISPRS Commission V Symp. 2006*, vol. 36, 2006.

[7] M. Hemmleb and J. Albertz, "Microtopography-the photogrammetric determination of friction surfaces," *International Archives of Photogrammetry and Remote*, vol. 33, pp. 56–63, 2000.

[8] M. A. Sutton, N. Li, D. Garcia, N. Cornille, J. J. Orteu, S. R. McNeill, H. W. Schreier, and X. Li, "Metrology in a scanning electron microscope: theoretical developments and experimental validation," *Measurement Science and Technology*, vol. 17, p. 2613, 2006.

[9] M. Ritter, T. Dziomba, A. Kranzmann, and L. Koenders, "A landmark-based 3d calibration strategy for spm," *Measurement Science and Technology*, vol. 18, no. 2, p. 404, 2007.

[10] A. C. Malti, S. Dembélé, N. Le Fort-Piat, P. Rougeot, and R. Salut, "Magnification-continuous static calibration model of a scanning-electron microscope," *Journal of Electronic Imaging*, vol. 21, no. 3, pp. 033 020–1, 2012.

[11] L. Cui and E. Marchand, "Calibration of scanning electron microscope using a multi-image non-linear minimization process," in *Robotics and Automation (ICRA), 2014 IEEE International Conference on*, 2014, pp. 5191–5196.

[12] M. D. Grossberg and S. K. Nayar, "A general imaging model and a method for finding its parameters," in *Computer Vision, 2001. ICCV 2001. Proceedings. IEEE International Conference on*, vol. 2. IEEE, 2001, pp. 108–115.

[13] S. Ramalingam and P. Sturm, "Minimal solutions for generic imaging models," in *Computer Vision and Pattern Recognition, 2008. IEEE Conference on*, 2008, pp. 1–8.

[14] P. Miraldo and H. Araujo, "Calibration of smooth camera models," *Pattern Analysis and Machine Intelligence, IEEE Transactions on*, vol. 35, pp. 2091–2103, 2013.

[15] J. Heikkila and O. Silvén, "A four-step camera calibration procedure with implicit image correction," in *Computer Vision and Pattern Recognition, 1997. Proceedings, 1997 IEEE Computer Society Conference on*, 1997, pp. 1106–1112.